Journal of Food Engineering 387 (2025) 112313

Contents lists available at ScienceDirect

Journal of Food Engineering

journal homepage: www.elsevier.com/locate/jfoodeng

Exploring puffed rice as a novel ink for 3D food printing: Rheological characterization and printability analysis

Bo-Ram Park [a], Junhee No [b], Hyeonbin Oh [a], Chan Soon Park [a], Kwan-Mo You [a,c,*], Legesse Shiferaw Chewaka [a,**]

[a] Department of Agro-Food Resources, National Institute of Agricultural Science, RDA, Wanju-gun, 55365, Republic of Korea
[b] Department of Food Science and Nutrition, Kyungpook National University, Daegu, 41566, Republic of Korea
[c] Institute of Food Science and Innovation, University of Chester, Chester, UK

ARTICLE INFO

Keywords:
3D printing
Buildability
Gelatinization
Puffed rice
Rheology
Viscoelasticity

ABSTRACT

This study introduces a novel approach by using puffed rice (PR) as a sustainable and innovative ink for 3D food printing. Due to gelatinization and dextrinization, PR saw notable water absorption and solubility gains, with a modest viscosity uptick from 39.2 to 49.9 RVU, sharply contrasting Native rice (NR)'s jump from 128.9 to 167.8 RVU, emphasizing PR's minimal retrogradation. Gelatinized rice (GR) demonstrates similar stability in viscosity changes as PR, yet it requires more water and extended processing times for gelatinization. Conversely, PR's puffing process, which eliminates the need for water, offers quicker preparation and notable environmental benefits. Rheological analysis at 25% PR concentration reveals an optimal balance of viscosity (η, 897.4 Pa s), yield stress (τ_y, 2471.3 Pa), and flow stress (τ_f, 1509.2 Pa), demonstrating superior viscoelastic properties that facilitate enhanced printability and shape fidelity. Texture Profile Analysis outcomes reveals that PR significantly enhances key textural properties including hardness, adhesiveness, and springiness at this specific concentration. These findings highlight PR's potential as an eco-friendly and efficient ink choice for 3D-printed food products, providing enhanced performance and sustainability compared to GR and NR.

1. Introduction

Integrating 3D printing into the food industry marks a significant evolution in manufacturing and design methodologies, particularly in creating intricate and customized food structures (Demei et al., 2022; Liu, Y. et al., 2018). Food 3D printing offers numerous advantages, such as customization, precise ingredient control, and intricate food design (Chen, J. et al., 2019; Guo et al., 2022; Teng et al., 2022; Zhang et al., 2022). Extrusion-based 3D printing is a widely investigated technique wherein edible ink is extruded through a nozzle as a filament, and 3D food structures are constructed layer by layer (Nijdam et al., 2021). For successful 3D printing, food ink should possess the shear-thinning property to ensure smooth extrusion and sufficient mechanical strength to maintain its shape (Lille et al., 2018; Zhang et al., 2022).

Utilizing conventional macronutrient sources like carbohydrates and proteins as 3D printing ink is limited by challenges such as inconsistent extrusion and unstable structures, which are primarily related to rheological properties, such as viscosity and viscoelasticity (Liu et al., 2017; Yang et al., 2017). Among these carbohydrate sources, rice stands out as a biodegradable and cost-effective option. However, the application of native rice (NR) in 3D printing has been hindered by limited water solubility and unfavorable rheological characteristics for 3D printing (Liu et al., 2017; Yulianingsih and Gohtani, 2019).

To address these limitations, a variety of modification techniques have been explored, including physical, chemical, and enzymatic methods, to alter the starch properties in rice (Liu et al., 2017; Maniglia et al., 2020; Ojogbo et al., 2020; Zia-ud-Din et al., 2017). Gelatinization processes, inducing interactions between starch and water, can transform rice starch into a gel-like structure conducive to 3D printing applications (Zeng et al., 2021). Chemical modifications, such as ozone treatment, have been utilized to oxidize starch, enhancing its suitability as 3D print ink by altering its molecular structure (Maniglia et al., 2019). Enzymatic modifications offer another avenue, altering starch molecule size and structure to improve printability by modifying glycosidic bonds (Gulzar et al., 2023). The exploration of carbohydrate-based inks, particularly through starch gelatinization, has also been a subject of considerable research (Chen, H. et al., 2019; Huang et al., 2019; Liu

* Corresponding author.
** Corresponding author.
E-mail addresses: yookm09@gmail.com (K.-M. You), lege1980@korea.kr (L.S. Chewaka).

https://doi.org/10.1016/j.jfoodeng.2024.112313
Received 9 February 2024; Received in revised form 25 August 2024; Accepted 6 September 2024
Available online 7 September 2024
0260-8774/© 2024 The Authors. Published by Elsevier Ltd. This is an open access article under the CC BY license (http://creativecommons.org/licenses/by/4.0/).

Abbreviations

η	Viscosity
NR	Native rice
G'	Storage modulus
GR	Gelatinized rice
G''	Loss modulus
PR	Puffed rice
τ_y	Yield stress
XRD	X-ray diffraction
τ_f	Flow stress
RVA	Rapid visco analysis

et al., 2017; Maniglia et al., 2019; Zeng et al., 2021). Despite significant advancements in 3D printing technology, the application of puffed rice as a printing ink remains largely unexplored. This oversight highlights a compelling opportunity to leverage the distinctive properties of puffed rice, which could lead to a novel ink formulation that satisfies the specific rheological requirements for successful 3D food printing.

Puffed rice (PR), crafted through a distinctive puffing process, undergoes a significant metamorphosis that differentiates it markedly from its original form. Unlike conventional heat-induced starch gelatinization, the explosion puffing technique exposes rice grains to a unique combination of high pressure and temperature. This specialized process rapidly heats the internal moisture of the grains, causing a phase change that significantly escalates the internal pressure (Lai and Cheng, 2004; Majzoobi and Farahnaky, 2021). As the pressure is suddenly released, the water within the grains evaporates almost instantaneously, leading to the expansion and porosity of the grains. This method not only modifies the rice's physical characteristics by enlarging its volume and decreasing its density but also prompts profound molecular alterations. These alterations primarily involve changes in the starch architecture, thereby improving the interaction with water and modifying the rice's rheological properties in ways that traditional heat gelatinization does not (Kumar and Prasad, 2018; Mariotti et al., 2006). The transformation endows puffed rice with distinctive physicochemical properties, such as an improved water-binding capacity and a unique rheological profile, setting it apart from native rice and conventional gelatinized starches (Lai and Cheng, 2004). In addition, explosion puffing is both sustainable and efficient, as it completely bypasses the need for water and significantly reduces preparation time compared to conventional gelatinization (Huang et al., 2018; Mariotti et al., 2006). Consequently, these characteristics could address issues typically associated with starch-based food inks, such as retrogradation and inconsistent extrusion, offering a novel approach to 3D printing inks.

Our study introduces puffed rice as an innovative 3D printing ink in this context. Distinct from traditional starch sources, puffed rice undergoes a unique gelatinization process, particularly suited for 3D food printing applications. This research explores the untapped potential of puffed rice, addressing a significant gap in the current literature. By examining its properties and applications, we aim to open new avenues in the sustainable and efficient production of 3D-printed food products, underscoring our findings' novelty and practical implications in food technology.

2. Material and methods

2.1. Materials

High-quality glutinous rice (Shindongjin variety) was obtained from the National Institute of Crop Science and the National Institute of Agricultural Science, Wanju, Jeolabuk-do, South Korea.

2.2. Sample pre-treatment

2.2.1. Native rice (NR) flour preparation

NR flour was prepared by grinding rice grains in a laboratory blender until a fine powder was obtained. The resulting flour was then sieved through a 250-μm mesh to ensure uniform particle size distribution.

2.2.2. Gelatinized rice (GR) flour preparation

GR flour was prepared following the method outlined by Chen et al. (2019a,2019b). Briefly, 100g of NR flour was thoroughly mixed with 300 mL of distilled water and heated at 60 °C for 1 h to induce gelatinization. The gelatinized mixture was subsequently freeze-dried to remove moisture and ground into a fine powder. The resulting GR flour was then sieved through a 250-μm mesh to obtain a uniform particle size.

2.2.3. Puffed rice (PR) preparation

Based on the method detailed by Huang et al. (2018), a revised explosion puffing process was applied to NR grain. We adjusted the moisture content of the rice to be within 13–14%. The grains were then heated in a pressurized expansion chamber set between 0.8 and 1.5 MPa for 70–80 s. At the end of this puffing phase, the chamber was swiftly opened, triggering a rapid pressure drop and causing the water within the rice grains to evaporate instantaneously. The puffed rice was then cooled to ambient temperature, finely ground, and sieved through a 250-μm mesh. The resulting flour was stored in sealed polyethylene bags in a desiccator with silica gel for later analysis and measurement.

2.3. Characterization of NR, GR, and PR

2.3.1. Scanning electron microscopy

Microstructural analyses were performed using the Scanning Electron Microscopes (SU8230, Hitachi, Tokyo, Japan). The samples were fractured in a dry state to expose the cross-sections. This technique was adapted based on the methodology outlined by Liu, Y. et al. (2018). Each sample was then mounted on SEM sample stubs using double-sided carbon tape. The stubs were cleaned with acetone to remove any contaminants, ensuring that the tape adhered properly to the samples. A thin layer of the sample was applied to the stubs and subsequently coated with platinum to enhance conductivity and image clarity, following the modified method by Mariotti et al. (2006). The samples were examined under SEM at magnifications of 50 × for overview and 500 × for detailed ultrastructural imaging. The microscope was operated at an accelerating voltage of 15 kV. Each image was captured with a photo time of 85 s to ensure adequate image resolution and contrast.

2.3.2. X-ray diffraction measurement

The crystal structures of samples were examined using an X-ray diffractometer (X-ray diffractometer, Empyrean, Panalytical, Netherlands). The following parameters were used: target: Cu-Kα; filter: Ni; full-scale range: 3000 cps; scanning speed: 8°/min; voltage: 40 kV; current: 30 mA. The crystal form and crystal strength were measured at a diffraction angle (2θ) of 40–5° and then compared. The relative crystallinity index was calculated using the Origin program (Origin 6.0 Professional, 1991; MA, USA) by dividing the area of the crystalline peaks by the total area of both the crystalline and amorphous peaks.

2.3.3. Water absorption index

The water absorption index was measured using the method proposed by Huang et al. (2018) with minor modifications. 0.5 g of the dry sample and 20 mL of distilled water were placed in a 50 mL centrifuge tube, stirred at room temperature for 1 h, and then centrifuged for 30 min at 8000 rpm in a centrifuge (Hanil Science Industrial Co., Supra 22K, Seoul, Korea). The supernatant was removed, and the weight of the precipitate was measured and calculated using the weight ratio of the initial sample.

2.3.4. Swelling power and solubility

The swelling power and solubility of the samples were measured following the method described by Mariotti et al. (2006) with minor modifications. A sample with a dry weight of 0.5 g was mixed with 20 mL of distilled water in a 50 mL falcon tube, shaken for 30 min at a constant temperature of 25 °C, and then centrifuged at 8000 rpm for 30 min. The supernatant was placed in a dried constant-weight dish and dried in an oven at 105 °C. The swelling power and solubility were calculated using the weight of the precipitated sample and the resultant value of the supernatant dried in a dry oven at 105 °C as follows.

$$\text{Swelling power (g/g)} = \frac{\textit{Weight of pricipitate}(g)}{\textit{Weight of initial sample}(g)} \quad (1)$$

$$\text{Solubility (\%)} = \frac{\textit{Weight of dried supernatant}}{\textit{Weight of intial sample}} \text{ x } 100 \quad (2)$$

2.3.5. Pasting properties

Adapting the approach from Liu et al. (2017), we modified the method for assessing the pasting properties of samples. We analyzed the pasting properties by utilizing a Rapid Viscosity Analyzer (RVA 4500, PerkinElmer, MA, USA) and in accordance with AACC method 61–02.01. For each test, 3.0 g of sample powder was combined with 25.0 mL of water in an RVA container. The stirring procedure involved an initial high-speed rotation followed by a slower, consistent speed for the remainder of the test. The temperature protocol included an initial hold, a precise heating cycle, a maintenance phase at peak temperature, followed by a controlled cooling process, and a final hold. The parameters measured included peak, trough, breakdown, final, and setback viscosities.

2.3.6. Rheological properties

The rheological properties of different concentrations (15–40%) of samples at 25 °C were measured by a Hybrid Rheometer (Discovery HR-3, DHR, TA Instruments, USA) using a parallel plate (diameter 25 mm) with a gap of 1 mm. Prior to testing, the excess material outside the plate was scraped off, and the exposed part was covered with silicone oil to provide additional protection against sample drying.

The apparent viscosity of samples was at shear rates ($\dot{\gamma}$) ranging from 1 to 1000 s^{-1} at room temperature. A strain sweep was first performed, where the strain was varied from 0.1 to 1000% at a constant frequency of 10 rad/s; the elastic modulus (G') and loss modulus (G'') were recorded as functions of the oscillation strain (%). Yield stress (τ_y) and flow stress (τ_f) were also calculated under the stress amplitude range 0.01–1000 Pa at a constant frequency of 10 rad/s. In separate experiments, for frequency sweep analysis, the angular frequency was varied from 0.1 to 100 rad/s, and all measurements were performed at a strain value of 0.1% (within the identified linear viscoelastic region).

Following the methodology outlined in Chen, J. et al. (2019), alternative strain sweep experiments were conducted, applying oscillatory strains of 1% (within the linear viscoelastic range) for 2 min, followed by 100% (exceeding the linear viscoelastic range) for an equivalent duration in each cycle, at a rate of 10 radians per second. This approach was utilized to examine the changes in viscosity in response to varying shear strains.

2.4. Application of PR for 3D printing

2.4.1. 3D printing process and evaluation of shape accuracy

In line with the approach described by Lee et al. (2019), 3D models of various shapes were generated in.stl file format using slicing software for 3D printing (Repetier-Host V2.1.6, Hot-World GmbH & KG, Willich, Germany). These models were then brought to life using a YOLILO 3D printer (YOLI-LAB Co., Ltd., Seoul, Korea) and PR. The printing process involved the use of a Luer lock syringe equipped with a 1.1 mm nozzle. We mixed the PR and GR powders with distilled water to reach the desired concentrations of 20%, 25%, 30%, 35%, and 40% w/v. The mixtures were then stirred thoroughly to ensure homogeneity and left to hydrate for 30 min at room temperature to allow for full water absorption. After hydration, the inks were loaded into a 60 mL syringe equipped. Approximately 50 mL of each prepared ink was used in the 3D printing trials to evaluate their printability and structural integrity. The 3D printing was carried out with specific settings: a 1.1 mm nozzle diameter, a first layer height setting of 1.1 mm, a 1.1 mm gap between each layer, full infill (100%), and a printing speed of the extruder head at 35 mm/s, all under ambient conditions (25 °C). Post-printing, the print quality was assessed immediately, focusing on aspects like dimensional accuracy, structural robustness, and the quality of the surface finish, using photographs of the printed items for reference.

2.4.2. Texture profile analysis

The textural characteristics of the printed objects made from different concentrations of PR ink were examined using a TA-XT-plus texture analyzer (Stable Micro Systems, UK) equipped with a P36/R probe (36 mm in diameter). The analysis was performed on cylindrical objects measuring 20 mm by 20 mm, utilizing a double compression cycle method. The parameters set for the test included a probe speed of 1 mm/s, a trigger force set at 5 g, a 30% compression of the original object height, and a 5-s pause between the two compressions. Each sample underwent this testing process three times, and the tests were conducted at a temperature of 25 °C.

2.5. Statistical analysis

The results of the triplicate measurements were presented as the mean ± standard deviation. An analysis of variance was conducted using XLSTAT software version 2019.2.2 (Lumivero, Denver, CO, USA), and differences at $p < 0.05$ were considered significant.

3. Results and discussion

3.1. Characteristics of PR powder

3.1.1. Microstructure of NR, GR and PR

Fig. 1A and B presents a stark contrast in the morphological characteristics of NR, GR and PR grains and their SEM imaging, respectively. The NR grains maintain a relatively smooth and compact structure, indicative of unaltered starch granules with densely packed molecular

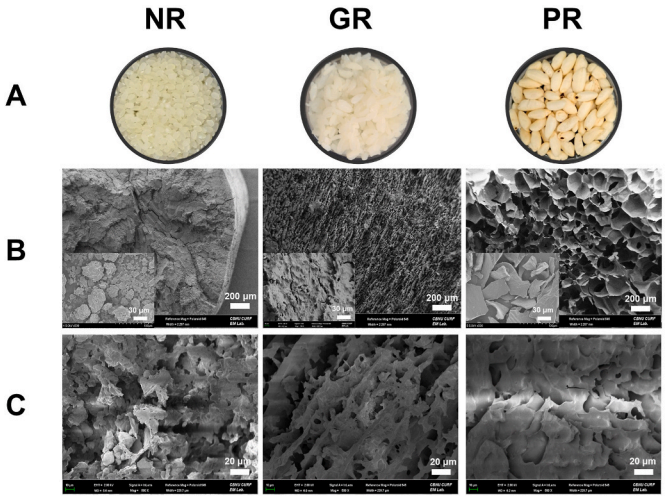

Fig. 1. Microstructural Variations of NR, GR, and PR in Different Forms; A) Displays the macroscopic appearances, SEM images B) Showing cross-sectional microstructures of grains (large images) and powders (insets), and C) Highlights the microstructure of 3D-printed gels.

arrangements. Meanwhile, GR samples, as evident from the granular details in Fig. 1B, show partially swollen granules with a slightly disrupted structure, typical of the gelatinization process (Liu et al., 2017). This process involves starch granules absorbing water and swelling, leading to a partial loss of crystallinity and molecular order, which, while useful in some applications, requires significant water input and extended processing times (Huang et al., 2018).

In contrast, PR displays a highly porous and expanded granules, resulting in internal structure fragmentation, characteristic of the physical changes induced by the explosion puffing process. This transformation is attributed to the explosion puffing process, where the grains are subjected to a rapid increase in temperature and pressure, leading to the instantaneous vaporization of bound-water within the starch matrix, causing the starch granules to rupture and resulting in the observed porous structure (Mariotti et al., 2006; Lee and Yang, 2020).

These morphological transformations in PR are crucial from a food engineering perspective. The increased porosity and internal structural disintegration, resulting from the explosion puffing process, enhance the starch's ability to interact with water, which is pivotal in 3D printing applications. This enhanced functionality makes PR particularly suited for 3D printing inks, offering superior resource efficiency and environmental benefits, key factors for industries aiming for rapid production cycles and material sustainability.

In Fig. 1C, the SEM images at 500× magnification illustrates distinctive characteristics across the rice gel samples. The gel derived from NR manifests a loosely compact inner structure, with clearly discernible rice starch granules suggesting minimal swelling. In contrast, the gels prepared from GR and PR display a markedly different appearance, indicating a more uniform and homogeneous inner structure. Particularly, the PR gel exhibits a more continuous and uniform structure compared to GR. This transition is primarily attributed to the formation of a gel network facilitated by gelatinized starch molecules upon hydration. However, PR's unique properties enhance printability and structural stability, making it a superior choice for sustainable 3D food printing technologies. Previous studies by Zheng et al. (2014) and Liu et al. (2017) have reported similar observations, where gelatinized rice starch exhibited continuous and porous aggregates, whereas native rice starch displayed smaller, angular, and polyhedral shapes.

3.1.2. X-ray diffraction

XRD is an effective tool to evaluate and quantify long-range crystalline structures in starch. The XRD patterns of NR, gelatinized rice (GR), and PR samples are shown in Fig. 2A. The NR showed strong diffraction peaks at 15.1°, 17.1°, 17.8°, and 23.2° (diffraction angle of (2θ)), which are typical A-type XRD patterns for cereal starch. This structure is characteristic of relatively unaltered starch granules found in natural rice (Kumar and Prasad, 2018; Kuo et al., 2019; Pathaw et al., 2023)

In contrast, GR and PR display diffraction patterns that deviate from the A-type crystallinity. The alteration in their XRD profiles suggests a transformation in the starch crystalline arrangement, likely due to the processes of gelatinization and puffing, respectively.

The XRD patterns of GR and PR show a significant reduction in the ordered crystalline structure of starch, with relative crystallinity indices of 3.58% and 10.30%, respectively, compared to NR, which has a relative crystallinity index of 33.04%. This reduction indicates a partial or complete loss of the crystalline regions in the starch granules. Gelatinization disrupts the crystalline structure due to the absorption of water and heat, which leads to the melting of these crystalline regions. Consequently, the starch exhibits an amorphous or V-type pattern, commonly associated with gelatinized starch (Pathaw et al., 2023; Zheng et al., 2022). The PR pattern deviates further from the NR, which can be associated with the dextrinization process during explosion puffing. Dextrinization is the thermal degradation of starch that leads to the breakdown of starch granules into shorter dextrin chains, resulting in a more amorphous structure and less defined XRD peaks (Lai and Cheng, 2004).

Explosion puffing involves subjecting the rice to high temperatures and pressures, leading to rapid water vaporization within the granules and causing them to expand (Huang et al., 2018; Kaur et al., 2023). This process not only gelatinizes the starch but can also cause dextrinization, further degrading the crystalline structure. The PR pattern with reduced peak intensity and increased amorphous halo suggests a higher level of degradation and loss of organized crystallinity than NR.

The XRD results imply that both gelatinization and puffing processes profoundly impact the crystalline integrity of starch in rice. The changes in crystalline to amorphous ratios could potentially affect the functional properties of the rice, such as water binding capacity, digestibility, and its interaction with other food components (Huang et al., 2018). This is especially relevant in food processing and 3D food printing, where the rheological properties and stability of starch-based materials are critical.

3.1.3. Comparison of physical properties between NR and PR

3.1.3.1. Water absorption index (WAI). Starch materials, including those used as 3D printing inks, benefit significantly from their water-retaining abilities (Zheng et al., 2022). As shown in Table 1, the WAI of PR flour (488.85%) is markedly higher than that of NR (177.02%) and GR (426.42%). This superior WAI in PR is due to its soft, rubbery, and highly porous matrix formed during the explosion puffing process (Lee and Yang, 2020; Mariotti et al., 2006). These results agreed with a previous report on the explosion puffing of cereals, which suggested that the absorption index of puffed rice was three times higher than that of native starch (Majzoobi and Farahnaky, 2021). The higher absorption

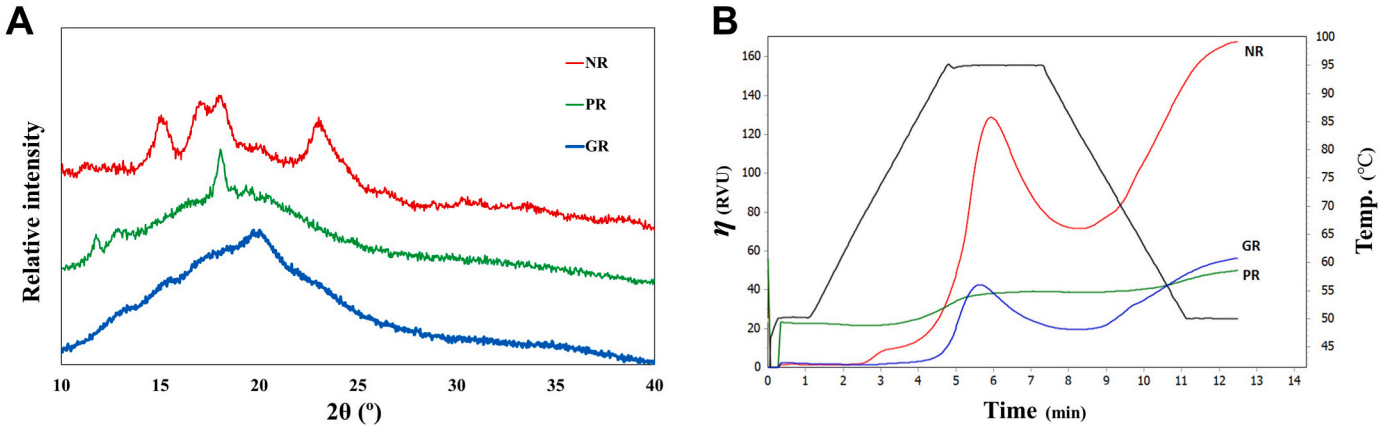

Fig. 2. A) X-Ray Diffraction Patterns and B) Pasting properties of NR, PR, and GR Samples.

Table 1
Comparison of the physical properties of NR,GR amd PR.

Samples	WAI (%)	Swelling power (g/g)	Solubility (%)
NR	177.02 ± 9.33^{c}	2.71 ± 0.05^{c}	3.33 ± 0.12^{c}
GR	426.42 ± 6.13^{b}	5.26 ± 0.06^{b}	8.15 ± 1.19^{b}
PR	488.85 ± 12.32^{a}	5.71 ± 0.08^{a}	10.13 ± 0.31^{a}

WAI: refers to water absorption index. All analyses were performed at room temperature. Values in the table are the mean ± std. dev. (n = 3). Different letters within a column represent significantly different means ($p < 0.05$).

index in PR and GR was also attributed to the disruption of the crystalline structure and gelatinization of starch, which allowed for the potential formation of hydrogen bonds with water molecules (Xu et al., 2021). Thus, while native starch granules are largely impermeable to water at room temperature, hindering their interaction with water molecules, GR and PR exhibit enhanced water interactions due to structural modifications. Gelatinization in GR partially disrupts starch granules, increasing water absorption compared to NR. However, the interaction of starch with water at higher temperature and pressure in explosion puffing leads to higher degree of gelatinization, not only disrupts granules but also breaks down the carbohydrate polymer structure, resulting in even higher water retention than GR (Huang et al., 2018; Fu et al., 2014; Severini et al., 2018). This significantly enhances the interaction between starch and water, making PR particularly advantageous for 3D printing applications at room temperature due to its superior water-binding capacity.

3.1.3.2. Swelling power and solubility. Native starch requires heating at elevated temperatures to initiate swelling and granule disintegration, limiting its use in applications that operate at ambient temperatures (Chen, H. et al., 2019). In contrast, PR flour exhibits a significant enhancement in swelling power, increasing from 2.71 (NR) to 5.71 g/g even at ambient temperatures (Table 1). This remarked improvement is attributed to the explosion puffing process, which structurally alters the starch granules, creating more porous structures and thereby increasing the material's capacity to absorb and retain water (Mariotti et al., 2006). The swelling capacity of GR also improves to 5.26 g/g, demonstrating the beneficial effects of starch modification. However, PR flour's unique structure, resulting from explosion puffing, optimizes it for 3D printing applications under ambient conditions, where enhanced material expansion without additional heating is particularly advantageous.

In addition, NR flour exhibits minimal water solubility (3.33%) at room temperature, rendering it less effective in forming gel or as a thickening or viscosifying agent (Severini et al., 2018). GR shows an improvement in solubility, reaching 8.15%, due to partial starch breakdown which increases water interaction. However, the structural transformation of rice starch via explosion puffing in PR goes further by leading to dextrinization and gelatinization without water (Lai and Cheng, 2004), resulting in a substantial increase in solubility to 10.13% (Table 1). This marked improvement over both NR and GR was due to the explosion puffing process, which significantly disrupts the granular structures and alters the molecular organization, enhancing the interaction between amylose and amylopectin molecules within the starch granules. This process promotes the loose association of hydrogen bonds during the induced gelatinization, as corroborated by several studies that observed similar phenomena in modified starches from different sources (Liu et al., 2017; Qiu et al., 2022; Majzoobi and Farahnaky, 2021; Xu et al., 2021).

Improved solubility at ambient temperatures is crucial for PR's application as a starch-based hydrogel in 3D printing, where enhanced hydration properties are essential for maintaining the structural integrity and functionality of printed objects. These hydration properties are closely related to the hydrophilic functional groups on the starch molecular chains and the gel network structure resulting from the puffing process (Qiu et al., 2022).

3.1.3.3. Pasting properties. The Visco-amylograph profiles depicted in Fig. 2B illustrate significant differences in the behavior of NR, GR, and PR during the rapid visco analysis (RVA) test. During the RVA test for NR, the viscosity exhibited a notable change: it increased to 128.9 RVU during gelatinization, then decreased to 57.4 RVU, followed by another increase to 167.8 RVU during the cooling phase. This pattern suggests typical starch behavior with temperature changes. In contrast, GR and PR demonstrate more stable profiles, indicating altered starch structures due to prior processing.

GR shows a more subdued response to heating, with a gradual increase and a more stable viscosity that does not exhibit the sharp peaks characteristic of NR. This behavior suggests that the gelatinization process has already partially broken down the starch structure, reducing its ability to swell and leach out upon further heating (Kumar and Prasad, 2018). PR, processed through explosion puffing, displays the most stable viscosity profile of the three, with minimal fluctuations from 39.2 RVU to 49.9 RVU.

This stability reflects the extensive disruption of the starch structure and further gelatinization induced by the high-temperature, high-pressure puffing process, that causes the moisture within the grain to vaporize rapidly, leading to the explosion of the kernel. This process disrupts the crystalline structure of starch, resulting in a partially or fully gelatinized material (Lee and Yang, 2020; Mariotti et al., 2006). Consequently, during the RVA analysis, PR displays a lower peak viscosity, which is indicative of the diminished integrity of the starch granules.

In 3D food printing, especially post-extrusion, one of the challenges is maintaining the shape and structure of the printed material (Hussain et al., 2022). The retrogradation of starch, which refers to the re-association of gelatinized starch molecules upon cooling, can lead to hardening or syneresis (water loss) (George et al., 2021), which may negatively affect the printed structure's stability and texture. Given that puffed rice shows a more stable viscosity profile with less pronounced peaks in gelatinization and retrogradation, it suggests that PR might exhibit less tendency to retrograde. Therefore, PR-based inks could potentially maintain a consistent texture and structure post-printing, providing a smoother and more predictable printing experience. This stability is beneficial in 3D food printing where precision and reliability are key.

In conclusion, the unique physical characteristics of PR, as a result of the explosion puffing process, could offer advantages for 3D food printing inks over NR and GR, promoting better shape retention and texture stability in the final printed products.

3.2. Rheological properties of rice gels for 3D printing

3.2.1. Flow properties

The study of the flow properties of rice gels, NR, GR, and PR, provides insightful distinctions in their rheological behavior, which are crucial for their use in 3D printing applications. The apparent viscosity and power-law model was applied to the flow properties of NR, GR and PR to quantify their rheological behavior in Fig. 3 and Table 2. When utilized as ink for 3D printing, it's crucial that the apparent viscosity is sufficiently low to facilitate smooth flow through a narrow nozzle yet high enough to ensure stable layering atop previously extruded layers (Chen, H. et al., 2019; Hussain et al., 2022).

The power-law model was applied to the flow properties of samples to quantify their rheological behavior. The model parameters obtained revealed distinct differences between samples.

$$\eta = K\dot{\gamma}^{n-1} \tag{3}$$

as evidenced by η, K, $\dot{\gamma}$, and n their respective viscosity (Pa•s), consistency index (Pa•s), shear rate (s^{-1}), and rate index. When the n-value equals 1, the material behaves as a Newtonian fluid. If $n < 1$, it exhibits shear-thinning properties, whereas $n > 1$ indicates shear-thickening

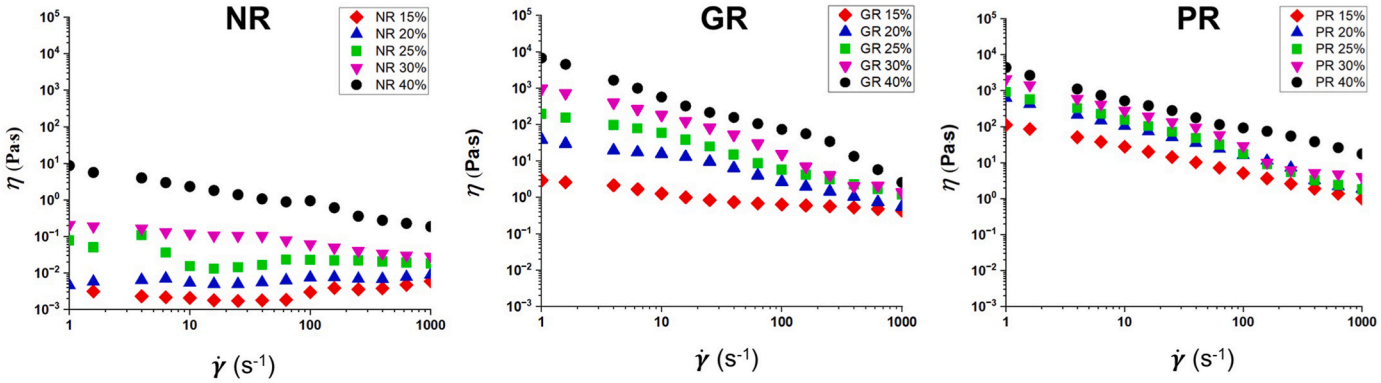

Fig. 3. Apparent viscosity (η) as a function of shear rate ($\dot{\gamma}$) of NR, GR and PR with 15 wt% (◆), 20 wt% (▲), 25 wt% (■), 30 wt% (▼), and 40 wt% (●).

Table 2
Flow properties of rice gels: A comparison between GR and PR.

	GR			PR		
Concentration	*n*	*K* (Pa.s)	R^2	*n*	*K* (Pa.s)	R^2
15%	0.98 ± 0.08^{a}	0.28 ± 0.12^{f}	0.150 ± 0.050^{b}	0.33 ± 0.02^{c}	111.75 ± 5.39^{f}	0.998 ± 0.001^{a}
20%	0.43 ± 0.01^{b}	36.43 ± 10.91^{f}	0.978 ± 0.009^{a}	0.19 ± 0.01^{e}	605.58 ± 27.49^{e}	0.996 ± 0.003^{a}
25%	0.27 ± 0.01^{d}	203.69 ± 16.70^{f}	0.992 ± 0.002^{a}	0.16 ± 0.01^{ef}	897.35 ± 81.45^{de}	0.992 ± 0.001^{a}
30%	0.10 ± 0.03^{fg}	1017.21 ± 23.74^{d}	0.982 ± 0.007^{a}	0.10 ± 0.02^{fg}	1522.98 ± 182.28^{c}	0.993 ± 0.003^{a}
40%	0.06 ± 0.02^{g}	5387.25 ± 69.29^{a}	0.996 ± 0.001^{a}	0.20 ± 0.02^{e}	3477.48 ± 664.09^{b}	0.995 ± 0.001^{a}

n: Flow behavior index; *K*: Consistency index; R^2: Coefficient of determination.
Values in the table are the mean ± std. dev. (n = 3). Different letters within a column represent significantly different means ($p < 0.05$).

behavior (Chandler, 2019).

NR exhibited a relatively uniform viscosity across various shear rates, especially at lower concentrations ranging from 15% to 30%, where the *n*-value approached 1.00, indicating near-Newtonian flow behavior. This consistency suggests that NR can maintain a steady flow through a nozzle, which is advantageous for certain printing applications. However, NR's inherent properties, particularly its limited ability to swell and dissolve, hindered the formation of a uniform gel mixture. Consequently, undissolved NR particles tended to float within the suspension, leading to non-homogeneous printing material. This issue was significant enough that data affected by low regression coefficients due to these inconsistencies were not presented in the results.

Both GR and PR, on the other hand, clearly stands out for its marked shear-thinning behavior across all concentrations except GR 15%, with *n*-values significantly below 1, detailed in Table 2. This substantial decrease in viscosity (η) with increased shear rate ($\dot{\gamma}$) indicates profound structural alterations due to the gelatinization or explosion puffing process, which enhance intermolecular interactions and contribute to a more cohesive gel network. The steep slopes depicted in Fig. 3 for PR and GR underscore their enhanced adaptability for 3D printing, where rapid adaptation to varying shear conditions is crucial. Furthmore, Table 2 showes a substantial increase in *K* (111.8–3477.5 Pa s) as PR concentration increases from 15% to 40%, illustrating a significant transformation in PR's rheological properties. In contrast, GR demonstrates a more gradual increase in *K* (0.28–1017.21 Pa s) up to 30% concentration. However, at 40% concentration, GR exhibits an extremely high viscosity of 5387.25 Pa s, which significantly surpasses the functional threshold for 3D printing inks.

These results indicate that the explosion puffing process significantly alters the rheological properties of rice, transforming it from a fluid with relatively low viscosity to one that is markedly more viscous and resistant to flow under the same shear conditions. The flow properties could be due to the combined effects of gelatinization and dextrinization of the starch granules during the puffing, shown in Figs. 1 and 2, which would result in a loss of granular integrity and an increase in molecular entanglement (Kumar and Prasad, 2018; Mariotti et al., 2006). Hence, the explosion puffing process can yield PR ink for 3D printing with dramatically different flow properties than NR and GR.

3.2.2. *Viscoelastic properties*

The stress and frequency sweep test for PR gel at varying concentrations (15%, 20%, 25%, 30%, and 40%) has yielded insightful results into the viscoelastic nature of PR. As depicted in Fig. 4A and **B**, the storage modulus (G'), represented by closed symbols, consistently surpassed the loss modulus (G''), denoted by open symbols, across all frequencies and concentrations tested. This dominance of G' over G'' is indicative of a solid-like behavior where elastic properties prevail over viscous ones, which is a desirable attribute for maintaining structural integrity during the 3D printing process (Fischer and Windhab, 2011; Tabilo-Munizaga and Barbosa-Cánovas, 2005).

Fig. 4A shows the corresponding stress sweep results of PR. It can be noticed that PR had higher G′ values corresponding to increasing the concentration. The detailed yield stress (τ_y) and flow stress (τ_f) values for each PR concentration are summarized in Table 3. With increasing PR concentration, τ_y value becomes crucial in supporting subsequently deposited layers and preserving the printed shapes during the deposition. In conjunction with our analysis of G', the τ_y values of PR starch were similarly affected by gelatinization and/or dextrinization of starch granules during the explosion puffing process. This transformation led to a disruption of granular integrity and an augmentation in molecular entanglement within the starch matrix. τ_f values represents the point at which G' equals G'', signifying the extrudability of a material during printing. This parameter indicates the force required for successful extrusion in the 3D printing process. From the τ_y and τ_f results, one can anticipate that higher concentrations present stronger mechanical properties, better printability, and higher resolution than lower concentrations, while 40% PR, which yielded a high τ_f value, struggling the stronger force is needed for the printing ink to be extruded from the

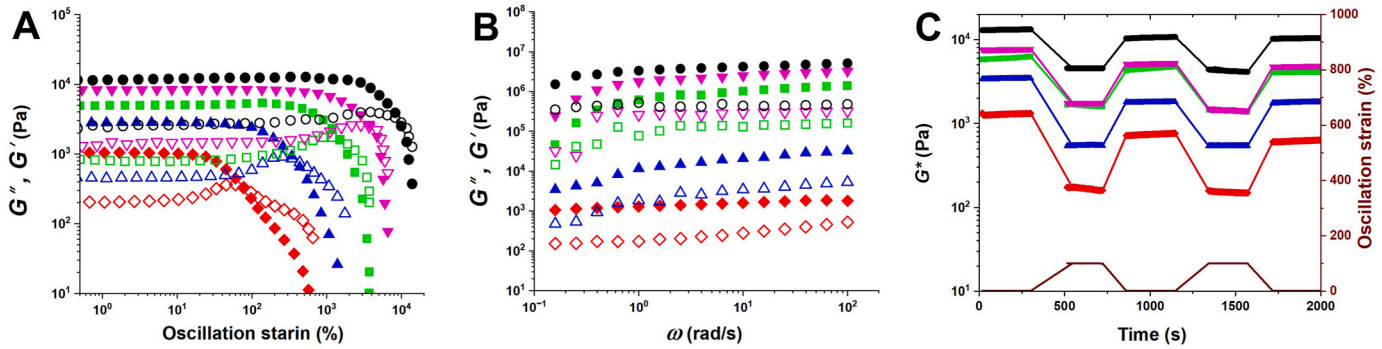

Fig. 4. Rheological Characterization of PR Paste for Extrusion-Based 3D Printing: A) Strain Sweep, B) Frequency Sweep, C) Alternating Strain Sweep Tests on 15 wt% (red), 20 wt% (blue), 25% wt% (green), 30 wt% (pink) and 40 wt% (black) of PR paste. Closed symbols = G', open symbols = G''. Alternating strain sweep was measured at 1 and 100% oscillatory strain cycle.

Table 3
Flow stress and yield Stress of PR paste at various concentrations.

PR	Flow stress, τ_f (Pa)	Yield stress, τ_y (Pa)
15%	73.023 ± 4.24^{c}	32.02 ± 3.75^{c}
20%	487.41 ± 112.77^{c}	298.25 ± 144.27^{bc}
25%	1509.21 ± 51.93^{c}	2471.27 ± 380.22^{b}
30%	3721.15 ± 405.10^{b}	5116.57 ± 449.40^{a}
40%	7337.30 ± 1962.75^{a}	6471.80 ± 2666.95^{a}

All analyses were performed at room temperature. Values in the table are the mean ± std. dev. (n = 3). Different letters within a column represent significantly different means ($p < 0.05$).

nozzle.

Fig. 4B presents the oscillatory frequency sweeps at a constant deformation and reveals that G' and G'' increase with higher angular frequency, a characteristic of materials with a strong gel structure. The fact that G' increased with frequency at all concentrations signifies that PR can form a stable gel network, less prone to deformation over time, a key factor for ensuring dimensional stability in printed constructs. The interplay between G' and G'' suggests that PR was capable of withstanding the shear forces applied during extrusion without compromising its ability to recover its shape post-deposition. This balance between G' and G'' is critical, as it affects the material's flow when subjected to force and its stability after deposition, influencing the resolution and accuracy of printed structures (Ji et al., 2022; Liu, Y. et al., 2018)

In comparison, GR at a 30% concentration, as detailed in Supplementary Fig. S1 and Table S1, displayed viscoelastic properties conducive to stable gel formation, suitable for 3D printing applications. Specifically, the rheological characterization demonstrated G′ of 20,286 Pa and a G'' of 2168.93 Pa at this concentration (see Fig. S1B), indicating its potential for gel formation but within a more restricted operational range compared to PR. While GR exhibits appropriate viscoelastic properties for printing at this concentration, it lacks the same level of adaptability and robust performance across broader concentration ranges as demonstrated by PR. This contrast is further emphasized by the τ_f of 728.44 Pa and τ_y of 466.78 Pa for GR at 30%, as shown in Table S1, which are significantly lower than the values observed for PR at similar or higher concentrations, underscoring PR's superior versatility and efficiency as a 3D printing ink, capable of adjusting to varying conditions and concentrations more effectively than GR.

Our observations of PR's rheological behavior are consistent with prior research on starches used in hot-extrusion 3D printing, reinforcing the applicability of these findings to 3D food printing applications (Chen, H. et al., 2019). These starch-based systems displayed similar trends, where increased starch concentration bolstered the material's viscoelastic properties, enhancing its suitability for extrusion-based printing. Therefore, the frequency sweep test results for PR indicate a material with significant potential for 3D food printing applications. The PR demonstrates a robust viscoelastic nature, with a high shape fidelity post-extrusion capacity, attributed to its enhanced gel strength.

3.2.3. *Alternate sweep test*

The printing medium extruded from the nozzle undergoes a high-shear process and a subsequent low-shear process (Hussain et al., 2022; Liu, Y. et al., 2018). As shown in Fig. 4C, all tested samples display a significant decrease in viscosity at high strains, followed by rapid recovery at low strains.

The complex modulus (G^*) displayed periodic fluctuations with oscillatory strain, indicating a reversible structure breakdown and build-up cycle. During periods of high strain, G^* decreased, suggesting the alignment or breakdown of the PR matrix. Upon the removal of high strain, the G^* increased as the PR structure exhibited recovery. This behavior is critical for 3D printing applications, where the material can flow under the shear strain and quickly regain elasticity to maintain shape post-extrusion.

In alignment with the theory of polymer conformational changes, flexible starch macromolecular chains orient themselves along the flow direction when subjected to external stress, reducing the system's conformational entropy. Upon the removal of this external force, there is a partial reinstatement of the conformational entropy (Chen, H. et al., 2019; Wang, 2017; Winnik and Yekta, 1997). Hence, Fig. 4C showed that the decrease in G^* across all concentration PR, when subjected to high shear strains, can primarily be attributed to the disassembly of the physical network. This disassembly is directly related to the realignment of the macromolecular chains. Following this, the swift increase in G^* at lower shear strains can be attributed to the quick rebuilding of the transient network. The partially or entirely reinstated conformation resulting from the reassembled physically entangled framework could enhance this rebuilding process. A similar pattern of alternating sweeps for gelatinized rice starch concentrations in the range of 10–30% was reported by Chen, H. et al. (2019), in which the G' showed a reversible nature for alternating sweeps of 1% and 100% strain.

The results suggest that PR, with its viscoelastic adaptability, is a promising material for extrusion-based 3D printing. It exhibits the requisite shear-thinning property for extrusion and rapid G^* recovery for shape retention, aligning with preferred material characteristics for 3D printing as described in literature on starch-based printing materials. Future work should focus on optimizing PR formulations to balance flow properties and structural stability, ensuring consistent printing quality. Adjusting PR concentrations or incorporating functional additives could enhance these properties, tailoring PR for specific printing requirements.

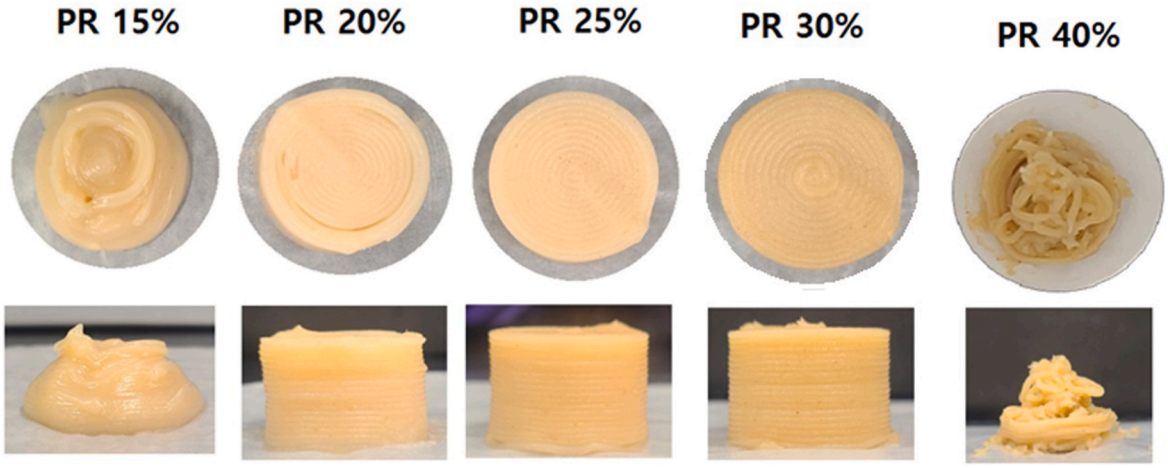

Fig. 5. Structures of extrusion-based 3D printing by PR paste (15, 20, 25, 30, and 40%), upper and side view (2 cm × 2 cm).

3.3. Printability assessment

3.3.1. Printing performance and shape accuracy

This study investigates the printability of PR as a 3D printing ink by correlating its rheological properties with printing performance, as illustrated in Fig. 5. At below-optimal concentrations (15% PR), the viscosity of the ink was too low (5.12 Pa s at a shear rate of 100 s^{-1}, whereas 20% PR was much higher at 16.8 Pa s), which led to significant deformations characterized by sagging and structural collapse. This occurred because the material lacked the viscoelastic properties necessary to support the structure's weight during the printing process.

In contrast, optimal concentrations (20–30% PR) provided a balance that allowed for smooth extrusion through the printer nozzle while maintaining enough rigidity to prevent deformation. At these concentrations, the viscosity was adequately balanced to facilitate quick solidification post-deposition, ensuring the material could support itself and maintain shape fidelity. The $\tau_{y,}$ 298–5116 Pa, at these concentrations was sufficiently high to prevent the layers from collapsing under their own weight, which is crucial for maintaining the overall structure during and after printing.

However, at supra-optimal concentrations (40% PR), the ink exhibited high viscosity which led to clogging and intermittent extrusion from the nozzle. This high viscosity (72.1 Pa s at a shear rate of 100 s^{-1}), coupled with excessive τ_f (7337.30 Pa), resulted in irregular layer stacking and the bulging of some sections of the structure. The G′ and G″ also play a critical role in these observations. At the optimal concentrations, the storage modulus dominated over the loss modulus, indicating that the material behaved more like a solid, which is essential for maintaining the shape against gravitational and vibrational forces during printing. The high storage modulus ensures that the material has sufficient elastic properties to support the layers above without flowing or deforming.

While similar tests on GR at around 30% concentration demonstrate its potential to achieve sufficient structural integrity for printing, it lacks the broader versatility of PR (Supplementary Fig. S2). Unlike PR, which adjusts well across a wide range of concentrations, GR's effectiveness is restricted to a narrower concentration window. This observation underscores PR's superior adaptability and efficiency as a 3D printing ink over GR, providing a sustainable and effective solution across various printing conditions.

These observations underscore the crucial role of rheological property equilibrium in determining successful printing outcomes and align with established theories in the literature. Studies by Chen, H. et al. (2019), Liu, Z. et al. (2018), and Zeng et al. (2021) have similarly highlighted the importance of a balanced rheological profile in 3D food printing. Specifically, these studies have demonstrated that the viscoelastic properties of the printing material must be finely tuned to achieve a delicate balance between fluidity for extrusion and solidity for structural integrity post-deposition.

Liu et al. (2018) found that approximately 53% w/v of rice flour was needed to achieve optimal printability in their study, highlighting the high material requirements for traditional rice-based inks. In contrast, our findings demonstrate that the explosion puffing process allows for effective 3D printing with much lower concentrations, as low as 25% w/v, significantly reducing the material needed while maintaining printability. This reduction not only lowers costs but also aligns with sustainable practices by minimizing resource use.

Additionally, while the detailed preparation process for GR described by Huang et al. (2019) involves multiple steps and additives to achieve desirable properties, our study shows that the explosion puffing process simplifies preparation by instantly gelatinizing the rice, thereby eliminating these resource-intensive steps. This results in a ready-to-use 3D printing ink without additional cooking or water, making it a more efficient option.

We have previously discussed how the puffing process enhances the rheological properties of rice, such as viscosity and elasticity, which are crucial for 3D printing applications. Compared to the methods in the literature, PR's optimized rheological profile at lower concentrations allows for less material use without compromising structural integrity. For example, at a concentration of 25% w/v, τ_y of PR was found to be optimal for maintaining the shape of printed materials, demonstrating that PR can provide the necessary structural support with reduced material input.

These superior rheological properties of PR allow for effective 3D printing with less material, enhancing efficiency and reducing waste. This not only demonstrates the practicality of using puffed rice as a 3D printing ink but also underscores its potential as a sustainable alternative in the field. Overall, the use of PR in 3D printing offers a promising solution that balances performance, efficiency, and sustainability.

3.3.2. Texture profile analysis

The Texture Profile Analysis (TPA) of 3D printed PR structures

Table 4
TPA profiles of printed objects using PR ink (20–30%).

Sample	Hardness (N)	Adhesiveness (mJ)	Springiness
PR 20%	1.28 ± 0.03^{c}	0.25 ± 0.03^{b}	0.09 ± 0.00^{c}
PR 25%	1.66 ± 0.04^{b}	0.25 ± 0.02^{b}	0.18 ± 0.01^{b}
PR 30%	3.33 ± 0.21^{a}	0.42 ± 0.09^{a}	0.27 ± 0.05^{a}

All analyses were performed at room temperature. Values in the table are the mean ± std. dev. (n = 3). Different letters within a column represent significantly different means ($p < 0.05$).

revealed pivotal mechanical characteristics varying with PR concentrations (20%, 25%, and 30%) in Table 4. These TPA parameters (hardness, adhesiveness, and springiness) were intricately related to PR concentration, influencing the buildability and structural integrity of the printed constructs.

At 20% PR concentration, the structures manifested the lowest hardness (1.28 N^{c}), suggesting a softer texture potentially undermining structural robustness. This aligns with a less pronounced rheological profile, which is evident in lower G' and τ_y and contributes to decreased buildability.

A concentration of 25% PR presented a marginal increase in hardness (1.66 N^{b}) and springiness (0.18^{b}), indicating a structurally firmer composition conducive to self-supporting layers in printing. The rheological data reflects the results, where increased G' and τ_y at this concentration correspond to the enhanced viscoelastic properties necessary for 3D printing. A similar correlation in hardness and G' was previously observed as solid and/or starch content increased (Anukiruthika et al., 2020; Maniglia et al., 2020). The springiness of the ink is a measure of its capacity to return to its original form following deformation, as highlighted by Du et al. (2022) and Ji et al. (2022). Furthermore, Du et al. (2022) demonstrated that adding NR to wheat dough reduces its viscoelastic properties due to NR's gluten-free nature, preventing the formation of a viscoelastic network and decreasing springiness. However, the PR material's springiness depended on its concentration, exhibiting a significant increase ($p \leq 0.05$) as the concentration rose. This demonstrates that PR's concentration distinctly improves its viscoelastic network formation, outperforming NR. This process capitalizes on PR's composition to enhance network robustness, demonstrating a refined method for boosting food products' textural qualities and printability. This correlation is further supported by alternative sweep data, indicating a consistent pattern of viscosity changes under different shear strains, as shown in Fig. 4C, highlighting the adaptability of PR's viscoelastic properties with concentration adjustments.

In discussing the impact of adhesiveness on the printability of PR-based inks for 3D printing, it is essential to define adhesiveness in the context of this study. Adhesiveness refers to the property of a material that causes it to stick, cling, or adhere to another surface (Anukiruthika et al., 2020). This property is particularly relevant in 3D printing, where the ink must maintain a delicate balance between adherence for layer stability and ease of flow through the printing nozzle. Interestingly, our findings indicate that the adhesiveness of inks with 25% PR concentration was as low as that observed in inks with 20% PR concentration, challenging the common expectation that higher concentrations would automatically lead to increased adhesiveness. As Anukiruthika et al. (2020) emphasized, excessive adhesiveness can impede ink flow through the nozzle, compromising printing efficiency and quality. Hence, inks with lower adhesiveness, like those with 20% and 25% PR concentration, are preferred for 3D printing, as they enable a smoother extrusion process, allowing for the precise creation of structures without undermining their integrity. Furthermore, the analysis of τ_f supports this result. Despite the incremental increase in PR concentration from 20% to 25%, there is no statistically significant difference in τ_f, underscoring a similar trend to adhesiveness. This lack of significant variation in τ_f, as shown in Table 3, coupled with the adhesiveness data, suggests a potential correlation between these two properties. The consistency in τ_f across these concentrations may indicate that modifying PR content can enhance specific mechanical properties, such as hardness, without adversely affecting the adhesiveness or flow resistance. This balance is critical in formulating 3D printing inks that are robust yet printable, offering a precise and controlled deposition of material.

However, at a 30% PR concentration, the τ_f increases substantially to 3721.2 Pa, indicating a higher resistance to flow under applied stress. This concentration also corresponds with increased hardness (3.33 N^{a}) and springiness (0.27^{a}), suggesting enhanced structural robustness and buildability. Due to its adhesiveness, it introduces challenges related to the extrusion process, which may hinder the material's ability to be extruded through the printing nozzle efficiently.

As the PR concentration rises, the starch molecules form more robust networks, resulting in a stronger gel (Fonseca-Florido et al., 2017; Liu et al., 2016). This heightened hardness and springiness are beneficial for 3D printing because it contributes to the durability and stability of the printed structure (Du et al., 2022), especially after the printing process is complete. It ensures that the layers of the printed object adhere to one another effectively, preventing delamination and maintaining the object's shape during and after printing. However, while increased hardness and springiness can improve the structural integrity of the printed object, it is essential to balance this property with the material's extrudability. Therefore, finding the optimal PR concentration is key to achieving a harmonious balance that leverages the increased hardness and springiness for structural benefits while allowing ink to flow adequately through the printing nozzle.

4. Conclusion

This study establishes that puffed rice is not only a viable and sustainable option for 3D food printing ink but also demonstrates superior rheological properties when compared to NR and GR. These advantageous properties are largely due to its enhanced water solubility and the significant transformation of NR's ultrastructure, which occurs during the explosion puffing process that involves high pressure and heat. These properties render PR particularly suitable for 3D food printing, as evidenced by the 3D printing accuracy and the TPA test results. The TPA tests corroborated the rheological findings, with a 25% PR concentration providing an excellent balance between printability and structural integrity. This specific concentration of PR ensures smooth flow through the printer nozzle and maintains the shape and texture of the printed product, making it the ideal formulation for 3D food printing applications. Importantly, the modified puffed rice material does not require any additional heating during the ink preparation process, unlike traditional methods that often necessitate cooking or gelatinization. This eliminates the need for heating, thereby simplifying the production process and reducing energy consumption, which further supports the sustainability of using puffed rice as a 3D printing ink. The explosion puffing process, which inherently gelatinizes the rice, allows PR to bypass issues of retrogradation, enhancing the material's stability and sustainability. These results contribute to the burgeoning field of food technology, positioning PR as a promising material for innovative 3D food printing applications.

Role of the funding source

The funders had no role in the design of the study; in the collection, analyses, or interpretation of data; in the writing of the manuscript; or in the decision to publish the results.

Declaration of generative AI in scientific writing

The author declares that there is no AI used in this article writing.

CRediT authorship contribution statement

Bo-Ram Park: Writing – original draft, Methodology, Funding acquisition, Conceptualization. **Junhee No:** Validation, Methodology, Data curation. **Hyeonbin Oh:** Methodology, Data curation. **Chan Soon Park:** Writing – review & editing. **Kwan-Mo You:** Writing – review & editing, Supervision. **Legesse Shiferaw Chewaka:** Writing – review & editing, Methodology, Investigation, Data curation.

Declaration of competing interest

The authors declare that they have no known competing financial interests or personal relationships that could have appeared to influence the work reported in this paper.

Data availability

Data will be made available on request.

Acknowledgments

This research was funded by the Research Program for Agricultural Science & Technology Development (Project No. PJ01728201) and the National Institute of Agricultural Science, Rural Development Administration, Republic of Korea.

Appendix A. Supplementary data

Supplementary data to this article can be found online at https://doi.org/10.1016/j.jfoodeng.2024.112313.

References

Anukiruthika, T., Moses, J., Anandharamakrishnan, C., 2020. 3D printing of egg yolk and white with rice flour blends. J. Food Eng. 265, 109691.
Chandler, H.D., 2019. A physical basis for non-Newtonian power-law viscosity. Soft Mater. 17 (2), 137–142.
Chen, H., Xie, F., Chen, L., Zheng, B., 2019. Effect of rheological properties of potato, rice and corn starches on their hot-extrusion 3D printing behaviors. J. Food Eng. 244, 150–158.
Chen, J., Mu, T., Goffin, D., Blecker, C., Richard, G., Richel, A., Haubruge, E., 2019. Application of soy protein isolate and hydrocolloids based mixtures as promising food material in 3D food printing. J. Food Eng. 261, 76–86.
Demei, K., Zhang, M., Phuhongsung, P., Mujumdar, A.S., 2022. 3D food printing: controlling characteristics and improving technological effect during food processing. Food Res. Int. 156, 111120.
Du, Y., Zhang, M., Mujumdar, A.S., Phuhongsung, P., Yang, C., 2022. Effect of addition of rice flour and yeast on improving 3D printing of fermented dough. J. Food Process. Preserv. 46 (11), e17016.
Fischer, P., Windhab, E.J., 2011. Rheology of food materials. Curr. Opin. Colloid Interface Sci. 16 (1), 36–40.
Fonseca-Florido, H.A., Gómez-Aldapa, C.A., Velazquez, G., Hernández-Hernández, E., Mata-Padilla, J.M., Solís-Rosales, S.G., Méndez-Montealvo, G., 2017. Gelling of amaranth and achira starch blends in excess and limited water. LWT–Food Sci. Technol. 81, 265–273.
Fu, Z.-q., Wang, L.-j., Zou, H., Li, D., Adhikari, B., 2014. Studies on the starch–water interactions between partially gelatinized corn starch and water during gelatinization. Carbohydr. Polym. 101, 727–732.
George, J., Nair, S.G., Kumar, R., Semwal, A., Sudheesh, C., Basheer, A., Sunooj, K.V., 2021. A new insight into the effect of starch nanocrystals in the retrogradation properties of starch. Food Hydrocolloids for Health 1, 100009.
Gulzar, S., Narciso, J.O., Elez-Martínez, P., Martín-Belloso, O., Soliva-Fortuny, R., 2023. Recent developments in the application of novel technologies for the modification of starch in light of 3D food printing. Curr. Opin. Food Sci., 101067
Guo, Z., Arslan, M., Li, Z., Cen, S., Shi, J., Huang, X., Xiao, J., Zou, X., 2022. Application of protein in extrusion-based 3D food printing: current status and prospectus. Foods 11 (13), 1902.
Huang, M.-s., Zhang, M., Bhandari, B., 2019. Assessing the 3D printing precision and texture properties of brown rice induced by infill levels and printing variables. Food Bioprocess Technol. 12, 1185–1196.
Huang, R., Pan, X., Lv, J., Zhong, W., Yan, F., Duan, F., Jia, L., 2018. Effects of explosion puffing on the nutritional composition and digestibility of grains. Int. J. Food Prop. 21 (1), 2193–2204.
Hussain, S., Malakar, S., Arora, V.K., 2022. Extrusion-based 3D food printing: technological approaches, material characteristics, printing stability, and post-processing. Food Eng. Rev. 14 (1), 100–119.
Ji, S., Xu, T., Li, Y., Li, H., Zhong, Y., Lu, B., 2022. Effect of starch molecular structure on precision and texture properties of 3D printed products. Food Hydrocolloids 125, 107387.
Kaur, R., Kumar, A., Kumar, V., Kumar, S., Saini, R.K., Nayi, P., Gehlot, R., 2023. Recent advancements and applications of explosion puffing. Food Chem. 403, 134452.
Kumar, S., Prasad, K., 2018. Effect of parboiling and puffing processes on the physicochemical, functional, optical, pasting, thermal, textural and structural properties of selected Indica rice. J. Food Meas. Char. 12, 1707–1722.
Kuo, C.-H., Shieh, C.-J., Huang, S.-M., Wang, H.-M.D., Huang, C.-Y., 2019. The effect of extrusion puffing on the physicochemical properties of brown rice used for saccharification and Chinese rice wine fermentation. Food Hydrocolloids 94, 363–370.
Lai, H.M., Cheng, H.H., 2004. Properties of pregelatinized rice flour made by hot air or gum puffing. International journal of food science & technology 39 (2), 201–212.
Lee, J.H., Won, D.J., Kim, H.W., Park, H.J., 2019. Effect of particle size on 3D printing performance of the food-ink system with cellular food materials. J. Food Eng. 256, 1–8.
Lee, N.-Y., Yang, J.H., 2020. Influence of partial gelatinization treatment on the quality changes of puffed rice. Preventive Nutrition and Food Science 25 (2), 225.
Lille, M., Nurmela, A., Nordlund, E., Metsä-Kortelainen, S., Sozer, N., 2018. Applicability of protein and fiber-rich food materials in extrusion-based 3D printing. J. Food Eng. 220, 20–27.
Liu, Y., Chen, J., Luo, S., Li, C., Ye, J., Liu, C., Gilbert, R.G., 2017. Physicochemical and structural properties of pregelatinized starch prepared by improved extrusion cooking technology. Carbohydr. Polym. 175, 265–272.
Liu, Y., Laohasongkram, K., Chaiwanichsiri, S., 2016. Effects of heat-moisture treatment on molecular interactions and physicochemical properties of tapioca starch. MOJ Food Processing & Technology 3 (3), 304–311.
Liu, Y., Liu, D., Wei, G., Ma, Y., Bhandari, B., Zhou, P., 2018. 3D printed milk protein food simulant: improving the printing performance of milk protein concentration by incorporating whey protein isolate. Innovat. Food Sci. Emerg. Technol. 49, 116–126.
Liu, Z., Zhang, M., Bhandari, B., Yang, C., 2018. Impact of rheological properties of mashed potatoes on 3D printing. J. Food Eng. 220, 76–82.
Majzoobi, M., Farahnaky, A., 2021. Granular cold-water swelling starch; properties, preparation and applications, a review. Food Hydrocolloids 111, 106393.
Maniglia, B.C., Lima, D.C., da Matta Júnior, M., Oge, A., Le-Bail, P., Augusto, P.E., Le-Bail, A., 2020. Dry heating treatment: a potential tool to improve the wheat starch properties for 3D food printing application. Food Res. Int. 137, 109731.
Maniglia, B.C., Lima, D.C., Junior, M.D.M., Le-Bail, P., Le-Bail, A., Augusto, P.E., 2019. Hydrogels based on ozonated cassava starch: effect of ozone processing and gelatinization conditions on enhancing 3D-printing applications. Int. J. Biol. Macromol. 138, 1087–1097.
Mariotti, M., Alamprese, C., Pagani, M., Lucisano, M., 2006. Effect of puffing on ultrastructure and physical characteristics of cereal grains and flours. J. Cereal. Sci. 43 (1), 47–56.
Nijdam, J.J., LeCorre-Bordes, D., Delvart, A., Schon, B.S., 2021. A rheological test to assess the ability of food inks to form dimensionally stable 3D food structures. J. Food Eng. 291, 110235.
Ojogbo, E., Ogunsona, E.O., Mekonnen, T.H., 2020. Chemical and physical modifications of starch for renewable polymeric materials. Materials Today Sustainability 7, 100028.
Pathaw, P.M.S., Bhattacharya, S., Mahanta, C.L., 2023. Properties of heat moisture treated red rice paddy and its puffed product. Cereal Chem. 100 (3), 784–797.
Qiu, Z., Zheng, B., Xu, J., Chen, J., Chen, L., 2022. 3D-printing of oxidized starch-based hydrogels with superior hydration properties. Carbohydr. Polym. 292, 119686.
Severini, C., Azzollini, D., Albenzio, M., Derossi, A., 2018. On printability, quality and nutritional properties of 3D printed cereal based snacks enriched with edible insects. Food Res. Int. 106, 666–676.
Tabilo-Munizaga, G., Barbosa-Cánovas, G.V., 2005. Rheology for the food industry. J. Food Eng. 67 (1–2), 147–156.
Teng, X., Li, C., Mujumdar, A.S., Zhang, M., 2022. Progress in extrusion-based food printing technology for enhanced printability and printing efficiency of typical personalized foods: a review. Foods 11 (24), 4111.
Wang, Z.-G., 2017. 50th anniversary perspective: polymer Conformation A pedagogical review. Macromolecules 50 (23), 9073–9114.
Winnik, M.A., Yekta, A., 1997. Associative polymers in aqueous solution. Curr. Opin. Colloid Interface Sci. 2 (4), 424–436.
Xu, F., Zhang, L., Liu, W., Liu, Q., Wang, F., Zhang, H., Hu, H., Blecker, C., 2021. Physicochemical and structural characterization of potato starch with different degrees of gelatinization. Foods 10 (5), 1104.
Yang, F., Zhang, M., Bhandari, B., 2017. Recent development in 3D food printing. Crit. Rev. Food Sci. Nutr. 57 (14), 3145–3153.
Yulianingsih, R., Gohtani, S., 2019. Dispersion characteristics of pregelatinized waxy rice starch and its performance as an emulsifier for oil-in-water emulsions: effect of gelatinization temperature and starch concentration. Food Hydrocolloids 95, 476–486.
Zeng, X., Chen, H., Chen, L., Zheng, B., 2021. Insights into the relationship between structure and rheological properties of starch gels in hot-extrusion 3D printing. Food Chem. 342, 128362.
Zhang, J., Li, Y., Cai, Y., Ahmad, I., Zhang, A., Ding, Y., Qiu, Y., Zhang, G., Tang, W., Lyu, F., 2022. Hot extrusion 3D printing technologies based on starchy food: a review. Carbohydr. Polym. 294, 119763.
Zheng, B., Tang, Y., Xie, F., Chen, L., 2022. Effect of pre-printing gelatinization degree on the structure and digestibility of hot-extrusion 3D-printed starch. Food Hydrocolloids 124, 107210.
Zia-ud-Din, Xiong, H., Fei, P., 2017. Physical and chemical modification of starches: a review. Crit. Rev. Food Sci. Nutr. 57 (12), 2691–2705.